Cardiac Dysfunction Promotes Cancer Progression via Multiple Secreted Factors

Lama Awwad and Ami Aronheim

ABSTRACT

Heart failure and cancer are the leading cause of deaths worldwide. While heart failure and cancer have been considered separate diseases, it is becoming evident that they are highly connected and affect each other's outcomes. Recent studies using experimental mouse models have suggested that heart failure promotes tumor progression. The mouse models used involve major irreversible surgery. Here, we induced heart hypertrophy via expression of activating transcription factor 3 (ATF3) in cardiomyocytes, followed by cancer cells' implantation. Tumors developing in ATF3-transgenic mice grew larger and displayed a more highly metastatic phenotype compared with tumors in wild-type mice. To address whether ATF3 expression or the cardiac outcome are necessary for tumor progression, ATF3 expression was turned off after cardiac hypertrophy development followed by cancer cell implantation. The tumor promotion phenotype and the enhancement of metastatic properties were preserved, suggesting that the failing heart per se is sufficient to promote tumor progression. Serum derived from ATF3-transgenic mice enhanced cancer cell proliferation and increased cancer cell metastatic properties *in vitro*. Using a cytokine array panel, multiple factors responsible for promoting tumor cell proliferation and the metastatic phenotype were identified. Interestingly, the failing heart and the tumor separately and simultaneously contributed to higher levels of these factors in the serum as well as other tissues and organs. These data suggest the existence of intimate cross-talk between the hypertrophied heart and the tumor that is mediated by secreted factors, leading to cancer promotion and disease deterioration.

Significance: This work highlights the importance of early diagnosis and treatment of heart failure prior to reaching the irreversible stage that can exacerbate cancer progression.

Introduction

Heart failure (HF) and cancer are the leading cause of death worldwide (1). While HF and cancer have been considered separate diseases, it is becoming evident that these are highly connected and affect each other's outcome at multiple levels (2, 3). Cardiac diseases and cancer share similar risk factors including environmental hazards, genetic predisposition, smoking, obesity, hyperlipidemia, sedentary lifestyle, diabetes, and aging (4–6). Cardiac hypertrophy has long been thought as a "tumor-like" growth that display similar molecular signals for cell proliferation, cardiac myocyte hypertrophy, and cell death and survival pathways (7). It is well established that cancer treatments that are directed toward cancer cell eradication also cause cardiomyocyte death (8–10).

Further studies have shown that patients with HF after myocardial infraction (MI) have an increased risk for developing cancer (11, 12). To study the possible mechanisms involved in the cross-talk between these two diseases, cardiovascular research converged with cancer research. Interestingly, a recent study has shown that MI in a mouse model for HF resulted in enhanced intestinal adenoma tumor load (13–15). Subsequently, tumor promotion phenotype was described for breast cancer model following MI (6, 16).

In another mouse model that mimics heart changes that occur following aortic stenosis (AS) in human patients revealed that early cardiac remodeling prior to HF promotes cell proliferation and metastasis seeding (17). Secreted factors and the immune system are considered to be part of a large network that connects various organs to inform their physiologic and pathologic state to maintain the organism's homeostasis (2, 6). Because the studies described above employed major surgery intervention to induce cardiac stress, we sought to study tumor progression in a transgenic mouse model that spontaneously develops cardiac hypertrophy (18). We used the activating transcription factor 3 (ATF3) transgenic model (designated thereafter ATF3-transgenic), developed in our lab, to induce cardiac hypertrophy and cardiac dysfunction (19). We followed tumor growth and metastasis phenotype in ATF3-transgenic mice. ATF3 is a transcription repressor from the basic leucine zipper family that plays a role in preserving cellular homeostasis following various stresses (20). *ATF3* is an immediate early gene found at the receiving-end of multiple stresses and growth stimuli including cardiac insults (21). In addition, patients with HF display high levels of ATF3 protein (22). While the exact role of ATF3 is of debate (23, 24), it is well documented that ATF3 expression in cardiomyocytes is sufficient to induce cardiac hypertrophy, heart fibrosis, and reduced cardiac contractile function (19, 25). Therefore, in ATF3-trangenic mice, cardiac hypertrophy occurs in the absence of surgery intervention (19). Transgenic mice with adult ATF3 expression were implanted with Lewis lung carcinoma and breast cancer cells in the flank and in the mammary fat pad, respectively. Tumors displayed increased tumor size and higher metastatic capabilities as compared with tumor developed in control mice. We suggest that the remodeled heart and cancer cells exhibit intimate cross-talk via multiple secreted factors. Revealing the mode of communication between organs in health and disease may provide new means to

Department of Cell Biology and Cancer Science, The Ruth and Bruce Rappaport Faculty of Medicine, Technion, Israel Institute of Technology, Haifa, Israel.

Note: Supplementary data for this article are available at Cancer Research Online (http://cancerres.aacrjournals.org/).

Corresponding Author: Ami Aronheim, Israel Institute of Technology, 7th Efron St. Bat-Galim, PO Box 9649, Haifa 31096, Israel. Phone: 972-4829-5454; Fax: 972-4829-5225; E-mail: aronheim@technion.ac.il

Cancer Res 2022;82:1753–61

doi: 10.1158/0008-5472.CAN-21-2463

better cope with multiple pathologic situations such as cardiac remodeling, HF, and cancer to improve patient outcomes (2, 3, 15).

Materials and Methods

All experimental protocols were approved by the Institutional Committee for Animal Care and Use at the Technion, Israel Institute of Technology, Faculty of Medicine, Haifa, Israel. Approval number IL-155–11–17. All study procedures are complied with the guidelines from of the NIH Guide for the Care and Use of Laboratory Animals.

Animals

All mice used were backcrossed to C57Bl6 background for over six generations. The ATF3-transgenic mouse model is the result of mating of two transgenic mice; the first, expresses the human influenza hemagglutinin (HA) fused to the human ATF3 under the control of the tetracycline activator (tTA) regulatory DNA elements. The second expresses the tTA transcription factor under the control of the αMHC promoter (αMHC-tTA), directing tTA expression to cardiomyocytes (26). The tTA protein binding to the promoter is regulated by doxycycline (tet-off system). Double transgenic mice containing both the αMHC-tTA and ATF3-transgenes are expressing the human ATF3 in cardiomyocytes and are designated thereafter ATF3-transgenic, while single transgenic were used as controls.

Breeding cages include mice harboring either ATF3-transgenic (19) or αMHC-tTA (27). Mating cages were maintained under regular chow supplemented with doxycycline (0.2 mg/mL, Sigma D9891) in the drinking water containing 5% sucrose to counteract the bitter taste of antibiotics. Mouse genotyping was performed as described previously (19).Upon weaning at three weeks of age, regular water was provided to allow ATF3-transgene expression in cardiomyocytes. Mice were euthanized by 0.1 mL i.p. injection per 20 gm mouse of a mixture containing ketamine 100 mg/mL and xylazine 100 mg/mL prior to sacrifice. Hearts, tumors, and lungs were collected for further analysis. Number of mice used in each experiment is indicated in the figure legends.

Cell culture

The PyMT cancer cells were kindly provided by Prof. Tsonwin Hai (Ohio State University, Columbus, OH). pyMT cells are murine breast carcinoma cell line that was derived from primary tumor-bearing transgenic mice expressing polyoma middle T under the control of the murine mammary tumor virus promoter (28). The LLC cell line was purchased from the ATCC (29). Both cell lines were tested on February 2021 by IDEXX BioAnalytics and found to be free of *Mycoplasma* and viral contamination. Cells were cultured in DMEM containing 10% FBS, 1% streptomycin and penicillin, 1% L-glutamine, and 1% sodium pyruvate at 37°C in humidified atmosphere containing 5% CO_2. Cancer cell implantation used at maximal passage number five.

Cancer implantation

PyMT cells (10^5 cells per mouse) were orthotopically injected into the back left side mammary fat pad. LLC cells (0.5×10^6 per mouse) were implanted subcutaneously into the flanks. Tumor size was measured using a caliper, and tumor volume was calculated with the formula: $\text{Width}^2 \times \text{Length} \times 0.5$. The humane endpoint is defined when the maximal tumor size reaches 1,500 mm^3, according to the Institutional Animal Care and Use Committee. An experimental pulmonary metastasis assay was carried out with PyMT cells injected into the tail vein (2×10^6 cells/mL, unless otherwise specified). Mice were sacrificed 10 days later (17).

Cell proliferation *in vitro*

PyMT or LLC cells were seeded in medium containing 10% FBS at a concentration of 2×10^4 cells/mL for 6 hours. After the cells were attached to the plate, medium was replaced with serum-free medium for overnight. Next, medium was replaced by either serum-free medium or supplemented with 10% FBS (positive control), mouse blood serum from either control or ATF3-transgenic mice for 48 hours. CellTiter-Glo Luminescent Cell Viability Assay Kit was used to measure cell viability according to the manufacturer's instructions. Luciferase activity was measured with a TD 20/20 luminometer (Turner Designs).

Echocardiography

Mice were anesthetized with 1% isoflurane and kept on 37°C heated plate throughout the procedure. Echocardiography was performed with a Vevo2100 micro-ultrasound imaging system (VisualSonics, Fujifilm) equipped with 13- to 38- MHz (MS 400) and 22- to 55-MHz (MS550D) linear array transducers. Cardiac size, shape, and function were analyzed using conventional two-dimensional imaging and M-mode recordings. Maximal left ventricular end-diastolic (LVDd) and end-systolic (LVDs) dimensions were measured in short-axis M-mode images. Fractional shortening (FS) was calculated with the following formula: FS% = [(LVDd-LVDs)/LVIDd]x100. FS value is based on the average of at least three measurements for each mouse.

RNA extraction

RNA was extracted from hearts and tumor using an Aurum total RNA fatty or fibrous tissue kit (no. 732–6830, Bio-Rad) according to the manufacturer's instructions. Next, cDNA was synthesized from 1,000 ng purified mRNA with the iScript cDNA Synthesis Kit (no. 170–8891, Bio-Rad).

Blood serum

Blood was obtained from the facial vein with a 4-μm sterile Goldenrod Animal Lancet (MEDIpoint, Inc). Blood was collected and allowed to clot at room temperature for 2 hours, followed by 15 minutes of centrifugation at 2,000 × *g*. Serum was immediately aliquoted and stored at −20°C for future use.

ELISA

Quantification of candidate secreted factors protein levels in the blood was performed with Mouse CTGF-Connective Tissue Growth Factor ELISA Kit (E-EL-M0340, Elabscience), Mouse Ceruloplasmin ELISA Kit (NBP2–82160, Elabscience, Novus Biologicals) and mouse Fibronectin ELISA Kit (E-EL-M0506, Elabscience) according to the manufacturer's instructions.

Quantitative real-time PCR

Quantitative real-time polymerase chain (qRT-PCR) was performed with Rotor-Gene 6000 (Bosch Institute, Sydney, Australia) with absolute blue SYBR Green ROX mix (Thermo Scientific AB-4162/B). Serial dilutions of a standard sample were included for each gene to generate a standard curve. Values were normalized to either Hsp90 or GAPDH expression levels for heart and tumor, respectively. All oligonucleotide sequences used are found in Supplementary Table S1.

Immunofluorescence staining

Tumors were fixed in 4% formaldehyde overnight, embedded in optimal cutting temperature solution, and was serially sliced at 10-μm intervals. Frozen tumor sections were stained for Ki67 (Abcam, ab16667) and counterstained with DAPI. Images were acquired with

3DHistech Pannoramic 250 Flash III (3DHISTECH Ltd). Each section was fully scanned; analysis was performed by person who was blinded to the experimental groups, five fields were chosen randomly and automatically analyzed with ImageJ software. For every dot plot of image analysis, each dot represents the mean of the values taken from five fields, derived from a single mouse.

Hematoxylin and eosin staining

Lungs were fixed in 4% formaldehyde overnight, embedded in paraffin subsequently serially sliced at 6-μm intervals, then mounted on slides. Hematoxylin and eosin (H&E) staining was performed according to the standard protocol. Images were acquired using 3DHistech Pannoramic 250 Flash III (3DHISTECH Ltd). Each lung section was fully scanned. The number and the area of metastatic lesions were calculated with CaseViewer software.

Fibrosis staining

Heart or tumor tissue was fixed in 4% formaldehyde overnight, embedded in paraffin, serially sectioned at 10-μm intervals, and then mounted on slides. Masson trichrome staining was performed according to the standard protocol. Images were acquired using 3DHistech Pannoramic 250 Flash III (3DHISTECH Ltd). Each section was fully scanned. The percent of the interstitial fibrosis was determined as the ratio of the fibrosis area to the total area of the heart/tumor section using Image Pro Plus software.

Invasion migration assay

PyMT cells (2×10^5 cells in 0.2 mL serum-free DMEM) were incubated with 10% serum of either ATF3-transgene or control. FBS (10%) served as positive control and medium without serum served as negative control. Cells were added to the top compartment of a Boyden chamber that was coated with either 50 μL Matrigel (BD Biosciences) for invasion assays or 100 μL fibronectin (10 μg/mL) for migration assays. After 16 hours, cells that migrated to the bottom filter were stained with crystal violet and counted under an inverted microscope (Leica DMIL LED, Leica Microsystems) per 200× objective field. At least five fields per chamber were analyzed. Three biological repeats of each experiment were performed. Number of cells per field were counted using ImageJ software.

Western blot analysis

Heart tissues were homogenized in RIPA buffer (PBS containing 1% NP-40, 5 mg/mL sodium deoxycholate, 0.1% SDS) supplemented with protease inhibitors cocktail (P-8340, Sigma Aldrich); 1 mmol/L DTT; 2 mmol/L PMSF; 20 mmol/L β-glycerolphosphate; 0.1 mmol/L sodium vanadate; 20 mmol/L PNPP; PhosStop- (catalog no. 04906837001, Roche). Homogenization was performed at 4°C using the Bullet Blender homogenizer (BBX24; Next advance Inc.) according to the manufacturer's instructions as previously described. Next, lysates were centrifuged at maximal speed for 10 minutes and supernatants were frozen at −70`°C. The proteins were then separated by 12.5% SDS-PAGE, followed by a transfer to a nitrocellulose membrane. Blots were blocked in 5% dry milk in PBS and washed three times for 5 minutes in PBS. The primary antibodies used: anti-α-tubulin (catalog no. T-9026 Sigma), anti-ATF3 (ab254268), and anti-HA (12CA5 mAb). Primary antibodies were detected using the corresponding HRP-conjugated secondary antibodies obtained from Sigma-Aldrich.

Cytokine array

Serum was obtained from tumor bearing either ATF3-transgene or control mice and applied (75 μL) to Proteome Mouse XL Cytokine Array filters (catalog no. ARY028) according to the manufacturer's instruction. The signal corresponding to each factor in the array was quantified by TotalLab software analysis. The level of expression of each protein on the array was calculated relatively to the value obtained for the positive control.

Statistical analysis

Data are presented as mean ±SD. All mice were included in each statistical analysis unless they were euthanized for humane reasons before the experimental endpoint. Experimental groups were blinded to the experimentalists during data collection. Animals were selected for each group in a randomized fashion. Number of mice in each experimental group is at least $n = 5$. Statistical significance of tumor volume was determined by two-way repeated-measures ANOVA followed by the Bonferroni posttest. Comparison between several means was analyzed by one-way ANOVA followed by the Tukey posttest. Comparison between two means was performed by two-tailed Student *t* test or Mann–Whitney *U* test. Analyses were performed with GraphPad Prism 7 software. Values of $P < 0.05$ were accepted as statistically significant.

Data availability statement

The data generated in this study are available upon request from the corresponding author.

Results

We sought to examine whether mice with cardiac remodeling in the absence of either MI-dependent HF or pressure overload–dependent cardiac remodeling is sufficient to promote tumor progression. Towards this end, we used a transgenic mouse model expressing HA-tagged human ATF3 in cardiomyocytes, resulting in cardiac hypertrophy, fibrosis, and heart dysfunction (19). ATF3-transgenic and control mice were implanted into the mammary fat pad of female mice with Polyoma middle T (PyMT cells) as a syngeneic orthotopic breast cancer model at eight weeks of age (**Fig. 1A**; ref. 28). The tumor in ATF3-transgenic mice grew significantly larger and heavier as compared with control mice, starting at day 16 post implantation until the humane endpoint (**Fig. 1B** and **C**). Cardiac function was assessed by echocardiography prior to sacrifice and fractional shortening (FS) was calculated. The FS of ATF3-transgenic mice was significantly lower as compared with the normal contractile function of control mice (Supplementary Fig. S1A). As expected, ventricles/body weight (VW/BW) ratio is higher in ATF3-transgenic mice as compared with control mice (Supplementary Fig. S1B). ATF3-transgenic mice displayed higher levels of hypertrophic gene markers (Supplementary Fig. S1C). Masson's trichrome staining of heart sections from ATF3-transgenic stained significantly stronger as compared with control mice (Supplementary Fig. S1D). This was accompanied by higher levels of fibrosis gene markers transcription as assessed by qRT-PCR (Supplementary Fig. S1E). Collectively, ATF3-transgenic mice display clear cardiac remodeling and cardiac hypertrophy hallmark phenotype. Tumor sections derived from ATF3-transgenic mice stained stronger by Masson's trichrome staining (**Fig. 1D** and **E**). In addition, the tumors derived from ATF3-transgenic mice displayed higher levels of fibrosis hallmark genes as compared with control mice (**Fig. 1F**).

To examine whether the increase in tumor size and weight is due to increased cell proliferation, we stained tumor sections with cell proliferation marker anti-Ki67 (**Fig. 2A**). Tumor sections derived from ATF3-transgenic mice stained significantly higher for cell

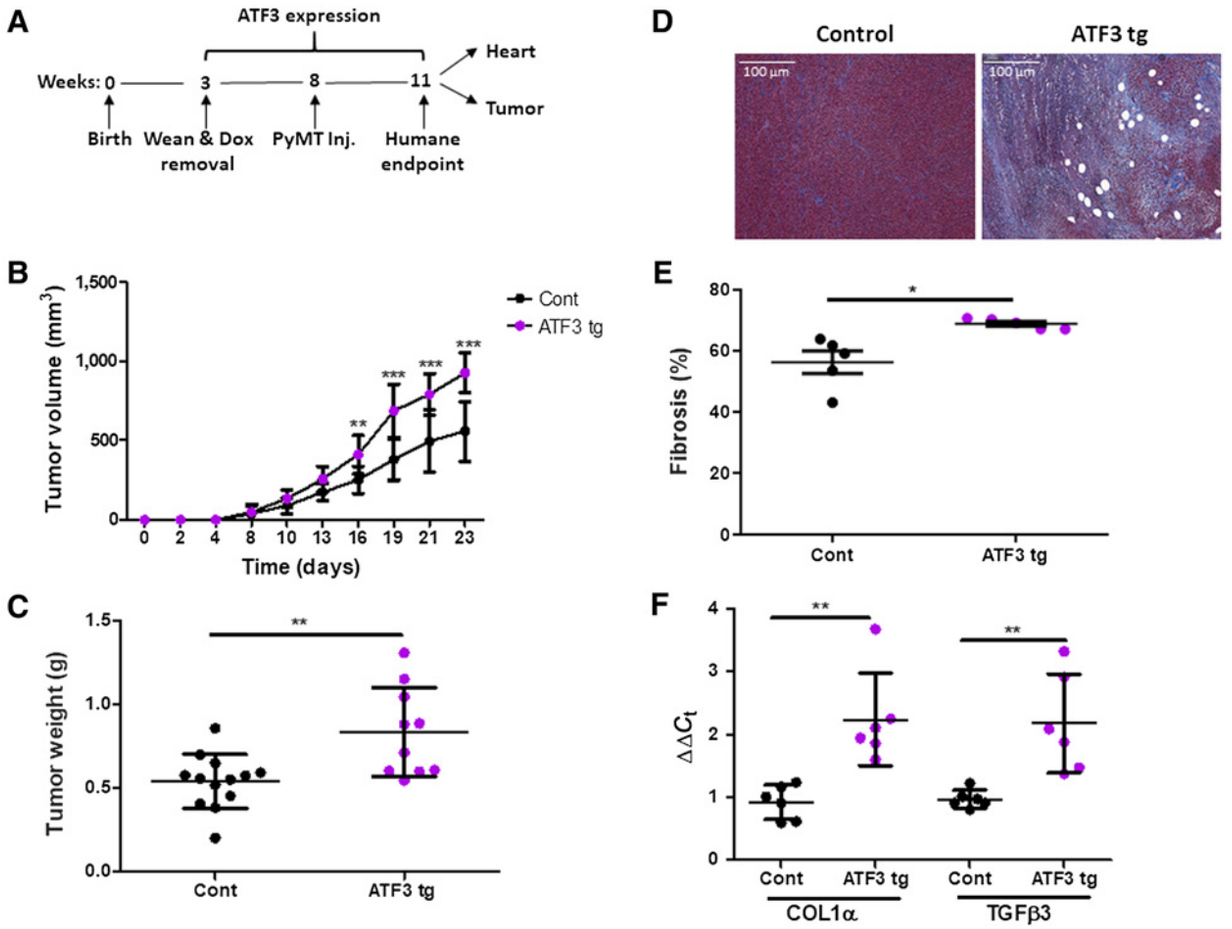

Figure 1.

Cardiac ATF3-transgenic promotes PyMT tumor progression. **A,** Schematic experimental timeline for polyoma middle T (PyMT) cancer cell model with female mice control (cont.; $n = 13$) or ATF3 transgenic (ATF3 tg.; $n = 10$). Doxycycline (Dox) was provided until weaning. Control and ATF3-transgenic were orthotopically implanted into the mammary fat pad with PyMT cells (10^5 cells per mouse). **B,** Tumor volume was monitored over time. **C,** Tumor weight at the endpoint. **D,** Representative images of tumor sections stained for Masson's trichrome. Scale bar, 200 µm. **E,** Quantification of the percent of the interstitial fibrosis. **F,** Tumor mRNA levels of the Collagen1α and TGFβ3 genes were measured by qRT-PCR, normalized to GAPDH housekeeping gene. Data are presented as relative expression compared with control determined as 1. Each dot represents one mouse. Data are presented as mean ±SD. Two-way repeated measures ANOVA followed by Bonferroni posttests (**B**), Student *t* test (**C** and **E**) or one-way repeated measures ANOVA followed by Tukey posttests. *, $P < 0.05$; **, $P < 0.01$; ***, $P < 0.001$.

proliferation per total cells as compared with tumor sections derived from control mice (**Fig. 2B**).

To test the role of putative secreted factor/s responsible for the increase in tumor cell proliferation mice serum was used to supplement serum-free culture medium of growing PyMT cells. Cells supplemented with serum obtained from ATF3-transgenic mice displayed higher cell proliferation as compared with control serum (**Fig. 2C**). Cell proliferation was alike in medium supplemented with either ATF3-transgenic serum or regular 10% FBS (**Fig. 2C**). Thus, we conclude that cardiac remodeling induced by ATF3 expression promotes tumor growth and cancer cell proliferation in the absence of pressure overload possibly via secreted factor/s. Tumor sections stained by H&E derived from ATF3-transgenic but not control tumors displayed invagination of cancer cells into the fatty tissue of the mammary fat pad (**Fig. 2D**). To study whether cancer cell invasiveness is due to serum-secreted factors as well, we used invasion and migration assay *in vitro* supplemented with mice serum. PyMT cells incubated with serum derived from ATF3-transgenic displayed higher invasion and migration properties as compared with serum derived from control mice (**Fig. 2E** and **F**).

To examine whether the tumor progression phenotype that occurs in ATF3-transgenic mice occurs in another cancer cell line, we used xenograft model for Lewis lung carcinoma (LLC) implanted in the flanks of eight weeks of age ATF3-transgenic and control male mice (Supplementary Fig. S2A). Tumor volume grew larger in ATF3-transgenic mice starting at day 18 until endpoint (Supplementary Fig. S2B). Cardiac function was lower and heart weight to body weight ratio was higher in ATF3-transgenic mice as compared with control mice (Supplementary Fig. S2C and S2D). Consistently with the results with PyMT cells, LLC tumors derived from ATF3-transgenic mice were significantly heavier than the tumors derived from control mice (Supplementary Fig. S2E). Finally, serum derived from ATF3-transgenic promoted LLC cell proliferation *in vitro* as compared with serum derived from control mice (Supplementary Fig. S2F).

We next sought to study whether ATF3-transgenic also induce the metastatic potential of cancer cells. Toward this end, we used

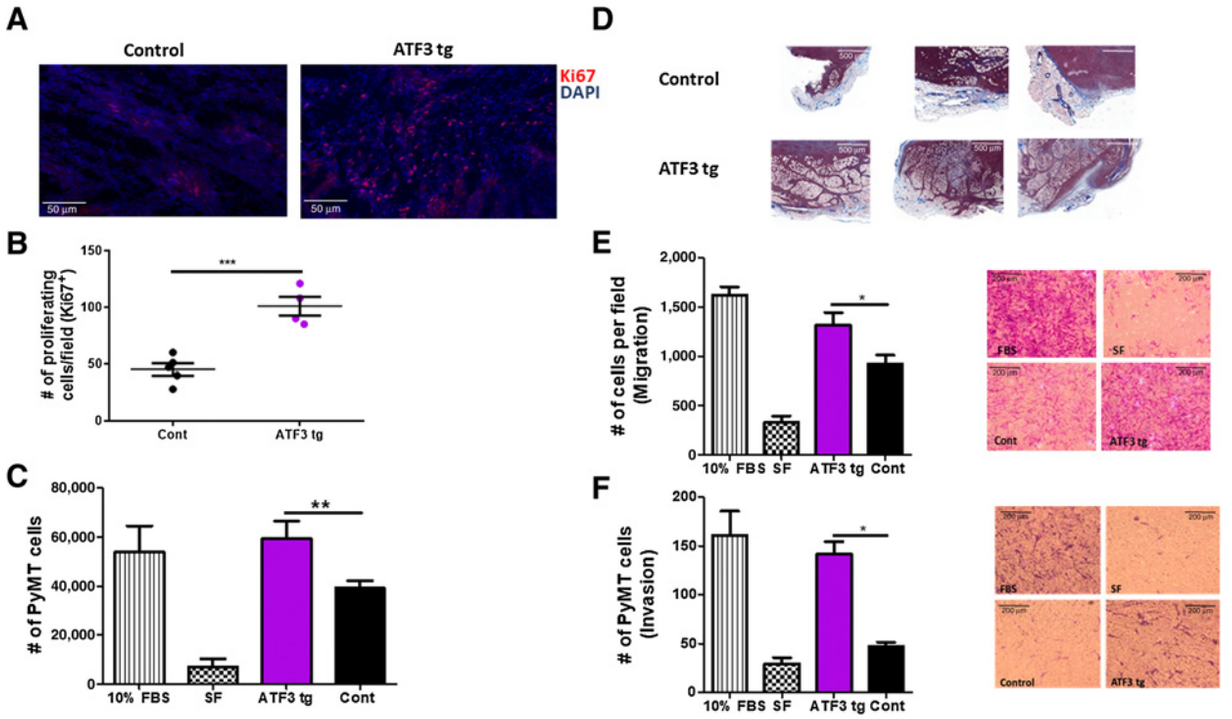

Figure 2.

Cardiac ATF3-transgenic promotes cancer cell proliferation. **A,** Representative image of PyMT tumor sections of control and ATF3-transgenic stained with anti-Ki67 (proliferating cells; red) and DAPI (nuclei; blue). Scale bar, 50 μm. **B,** Quantification of the number of proliferating cells in tumor section field. Each dot represents the mean of five fields in tumor section derived from a single mouse ($n = 4$ mice each) **C,** PyMT cells were cultured for 48 hours in the absence or supplemented with 10%: FBS, mouse blood serum drawn from either control or ATF3-transgenic. Proliferation was measured by Luminescent Cell Viability Assay kit using serum derived from at least three mice per group ($n = 4$ wells per treatment). **D,** Tumor sections derived from either ATF3-transgenic or control mice ($n = 3$ mice per group shown). Scale bar, 200 μm. **E** and **F,** Migration (**E**) and invasion (**F**) of PyMT cells assessed by Boyden chamber assays in the presence of fibronectin or Matrigel, respectively. Representative images are shown. Scale bar, 200 μm. Cell coverage was quantified from the images ($n = 5$–8 fields/group). Data are presented as mean ± SD. Student *t* test (**B**) or one-way repeated measures ANOVA followed by Tukey posttests (**C**, **E**, and **F**). *, $P < 0.05$; **, $P < 0.01$; ***, $P < 0.001$.

pulmonary experimental metastasis assay. Mice were sacrificed 10 days following cancer cell injection (**Fig. 3A**). H&E lung sections derived from ATF3-transgenic mice displayed more metastatic lesions that were also larger in size as compared with lungs sections derived from control mice (**Fig. 3B–D**).

Collectively, adult ATF3 expression in cardiomyocytes results in cardiac remodeling, cardiac hypertrophy, fibrosis, and contractile dysfunction. Cancer cells implanted in ATF3-transgenic mice grew larger in size and weight with increased cell proliferation, enhanced invasive capacity, and had higher level of fibrosis. Serum derived from ATF3-transgenic mice enhanced cancer cell proliferation, migration, and invasion properties *in vitro* as compared with control serum.

One of the questions that arise is whether the cancer progression effect observed is dependent on ATF3 expression. To examine this, ATF3 expression was turned-off by doxycycline supplementation at seven weeks of age followed by PyMT implantation at eight weeks of age (**Fig. 4A**). ATF3-transgene expression was significantly reduced following doxycycline addition as verified by both qRT-PCR and Western blotting using appropriate primers and antibodies, respectively (Supplementary Fig. S3A–S3C).

Clearly, the hearts derived from ATF3-transgenic that were treated with doxycycline for four weeks preserved their cardiac remodeling phenotype, that is, increased ventricles to body weight ratio (Supplementary Fig. S3D).

The potentiation of the cancer progression phenotype was preserved despite the fact that ATF3-transgene was no longer expressed (**Fig. 4B–D**).

Similarly, the increase of cancer cells seeding to the lungs was independent on continuous ATF3 expression (Supplementary Fig. S4A–S4D).

Previous studies as well as results herein suggest that the communication between the failing heart and the tumor occurs via serum-secreted factors. To identify these factors, we probed proteome profiler cytokine array with serum derived from tumor-bearing either ATF3-transgenic or control mice. Multiple cytokines and secreted factors were found at significant levels and with at least >2-fold higher levels in the serum of tumor-bearing ATF3-transgenic mice (**Fig. 5A**).

Previous studies suggested the possible involvement of secreted factors in failing heart following MI (13) and remodeled heart following transverse aortic constriction (TAC; ref. 17). Because the proteome array does not include all these factors, we examined the serum of some of the missing factors by ELISA. This analysis identified ceruloplasmin, connective tissue growth factor (CTGF), and fibronectin, to be elevated in the serum derived from ATF3-transgenic mice (**Fig. 5B**).

Multiple tissues may be responsible for the expression of the factors that were identified in the serum. Therefore, we measured the mRNA levels of the secreted factors in the hearts and the tumors

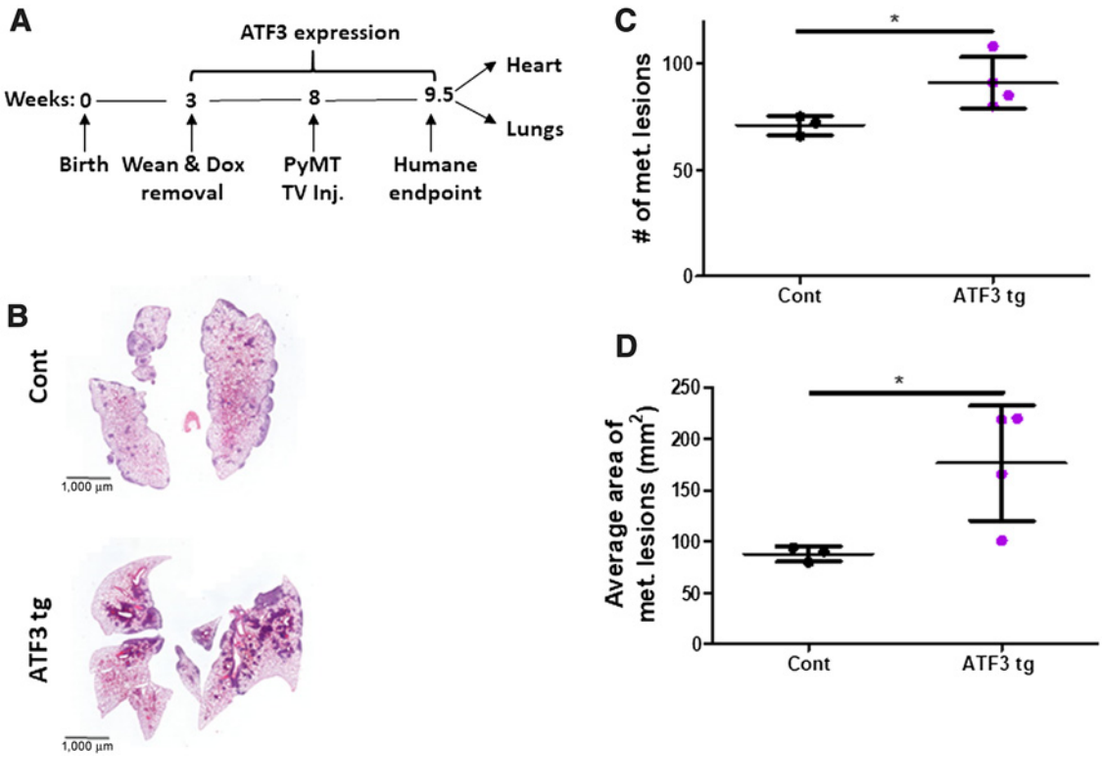

Figure 3.

Cardiac dysfunction enhances cancer cell colonization to the lungs in ATF3-transgenic mice model. **A,** Schematic experimental timeline for ATF3-transgenic and control mice followed by PyMT cell pulmonary experimental metastasis assay by tail vein injection (TV Inj.) of 2×10^6 cells per mouse; Control (Cont.; $n = 3$) or ATF3-transgenic (ATF3 tg.; $n = 4$) female mice. **B,** Representative image of lung sections stained with H&E. Scale bar, 1,000 μm. **C,** Number of metastatic lesions in the lungs. **D,** Average area of the metastatic lesions. Data are presented as mean ±SD. Student *t* test. *, $P < 0.05$.

derived from ATF3-transgenic and control mice (**Fig. 5B** and **C**). Interestingly, we identified factors that are expressed at higher levels specifically in the hearts of ATF3-transgenic mice as compared with control mice (these include: IGF1, periostin, ceruloplasmin, and Serpin E1; **Fig. 5C** and **D**, red bars). In contrast, some factors are expressed at higher levels exclusively in the tumors derived from ATF3-transgenic mice as compared with controls (these include: angiopoietin2, angiopoietin like-3, chitinase 3 like 1; **Fig. 5C** and **D**, black bars). In addition, the mRNA of VCAM, MMP9, CTGF, and fibronectin have been found to be expressed at elevated levels in both hearts and tumors derived from ATF3-transgenic mice (**Fig. 5C** and **D**, light blue bars). Moreover, the mRNA levels of cystatin C and E-selectin were not elevated neither in the heart nor in the tumor (**Fig. 5C** and **D**, green bars). This suggests that other tissues/organ expressing these factors at elevated levels in ATF3-transgenic mice as compared with control mice. Previous study suggested that SerpinA3 plays a key role in promoting cancer progression following MI and proliferation of colon cancer cells *in vitro* (13). Consistently, mRNA levels of SerpinA3 were found at significantly higher levels in the hearts derived from ATF3-transgenic mice (Supplementary Fig. S5A and S5B).

Collectively, ATF3-transgene expression in cardiomyocytes elicits a vicious cycle that results in hypertrophied heart, fibrosis, and cardiac dysfunction. Increased levels of multiple factors secreted by the heart, tumor and other organs mediate the promotion in tumor cell proliferation and potentiate their tumor metastatic phenotypes.

Discussion

Tissues and organs in the body are found in a constant cross-talk during normal growth as well as in pathological situations. Although, much focus is made to treat the diseased organ, the organism homeostasis is perturbed and therefore a wider holistic approach needs to be considered. It is well established that patients with HF due to either myocardial infraction or aortic stenosis have higher risk to develop cancer (12, 13, 17, 30). Recent studies demonstrated an unique cross-talk between the failing heart and tumor (13, 16, 17). Using mice models for pressure overload (TAC) and HF (MI), secreted factors were found to play key role in tumor promotion via either direct or indirect mechanisms. The former represents secreted factors that promote cell proliferation (17). Alternatively, the indirect effects are mediated via monocyte epigenetic switch in the bone marrow, resulting in an immunosuppressive phenotype (16). It is hypothesized that the indirect effects are mediated as well by secreted factors, which impose the monocytes "education" in the bone marrow. Previous studies suggested that HF effects on cancer cells are not generic, and it is dependent on the type of cancer (31). Whether or not HF and tumor cross-talk is dependent on the pathophysiologic basis leading to heart HF is questionable. Mice models for HF and pressure overload requires irreversible surgeries, therefore, it was impossible to distinguish between whether the cause or the HF outcome are responsible for promoting the tumor phenotype. To overcome this, in the MI model, the failing heart was transplanted to naïve mice and was connected to the circulation (13). This enabled to prove that HF-dependent secreted

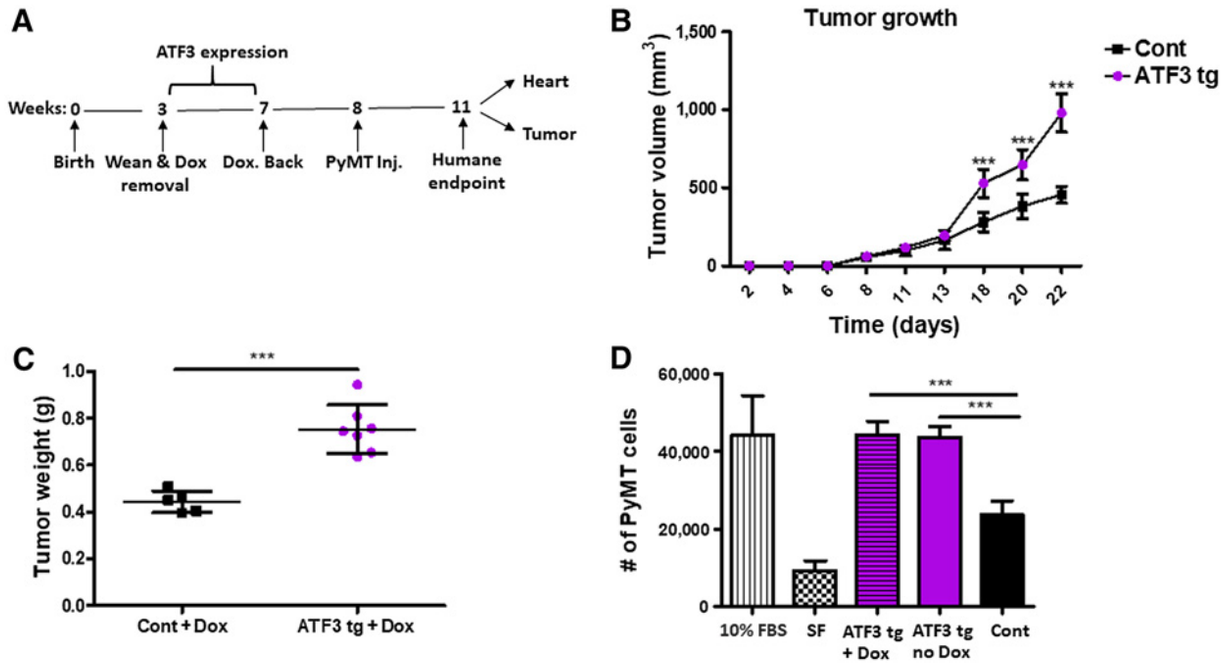

Figure 4.

Tumor promotion phenotype is independent on continuous ATF3-transgene expression. **A,** Schematic experimental timeline for PyMT cell model with control (cont.; $n = 5$) or ATF3-transgenic (ATF3 tg.; $n = 7$) female mice. Doxycycline (Dox) was removed at 3 weeks of age and was added back at 7 weeks of age. PyMT cells were injected one week later. Mice were sacrificed at humane endpoint. **B,** Tumor volume was monitored over time. **C,** Tumor weight at the endpoint. Each dot represents one mouse. **D,** PyMT cells were cultured for 48 hours in serum-free medium in the absence or supplemented with 10%: FBS, mouse blood serum drawn from either control or ATF3-transgenic. Proliferation was measured by Luminescent Cell Viability Assay using serum from at least three mice per group ($n = 4$ wells per treatment). Data are presented as mean ±SD. Two-way repeated measures ANOVA followed by Bonferroni posttests (**B**), Student *t* test (**C**), or one-way repeated measures ANOVA followed by Tukey posttests (**D**). ***, $P < 0.001$.

factors are responsible for tumor promotion. In the TAC model, a mouse strain resistant to cardiac remodeling failed to promote tumor growth (32). Thus, we concluded that cardiac remodeling per se is required for promoting tumor progression (17). Here, we employed an ATF3-transgenic mouse model to induce cardiac remodeling and heart hypertrophy. The advantages of the transgenic model are dual; the first is that cardiac remodeling occurs in the absence of any surgery intervention or hemodynamic alterations. The second, the cause for the cardiac-specific effects, that is, cardiac ATF3 expression, is reversible and can be turned off by doxycycline supplementation in the diet. The model includes two phases; the first is an initiation phase in which the ATF3-dependent gene expression program is induced prior to the cardiac phenotype, and the second phase, a cardiac remodeling gene program is activated and includes hallmark genes responsible for fibrosis, inflammation, cardiac hypertrophy, and HF (19). The ATF3-transgenic mouse model enabled us to examine whether tumor promotion phenotype requires continuous ATF3 expression or once the cardiac remodeling gene program is initiated, it is sufficient to provoke tumor promotion phenotype. Our results clearly show that once heart function is irreversibly deteriorated, the tumor progression occurs even in the absence of continues ATF3-transgene expression. Cardiac remodeling is known to result in an irreversible vicious cycle (33, 34) that is mediated by secreted factors and continues expression of endogenous ATF3 expression in the heart, leading to a tumor progression phenotype.

Using a proteome cytokine array, we have identified multiple factors that are present at higher levels in the serum derived from ATF3-trangenic mice that altogether contribute to the increased proliferation and migratory properties of cancer cells. The following factors have already been shown to play a role in promoting tumor progression: chitinase 3-like 1 (35), angiopoietin 2 (36), angiopoietin like-3 (37), E-selectin (38), MMP9 (39), IGF1 (40), cystatin C (41), CTGF (42), periostin (43), and SerpinA3 (44). Although it was expected that the failing heart will be the main source of synthesis of these factors, we found that some of these factors are highly expressed in both the tumor and the heart simultaneously. Furthermore, some factors are exclusively expressed in the tumor. In contrast, the expression of cystatin C a renal biomarker (45) and E-selectin a cell adhesion molecule on endothelial cells (38) is neither attributed to the heart nor to the tumor. These factors may be secreted by the kidneys and endothelial cells, respectively. Therefore, we conclude that an intimate cross-talk between the heart and the tumor is responsible for the overall cancer outcome and the failing heart. In addition, we highlight the possible contribution of other tissues and organs to the tumor promotion phenotype via factors secreted in a paracrine fashion.

Chronic stress is known to promote cancer development via the activation of the neuroendocrine system (46, 47); however, here we showed that a direct communication occurs between the remodeled heart and the tumor through the secretion of multiple factors to the blood that promotes tumor progression.

The current study focused on the heart and the tumor; however, we cannot exclude the recruitment of the immune system to the heart, tumor and/or both. In addition, previous studies showed that HF affects the metabolism in other organs such as the liver, β-cells, and

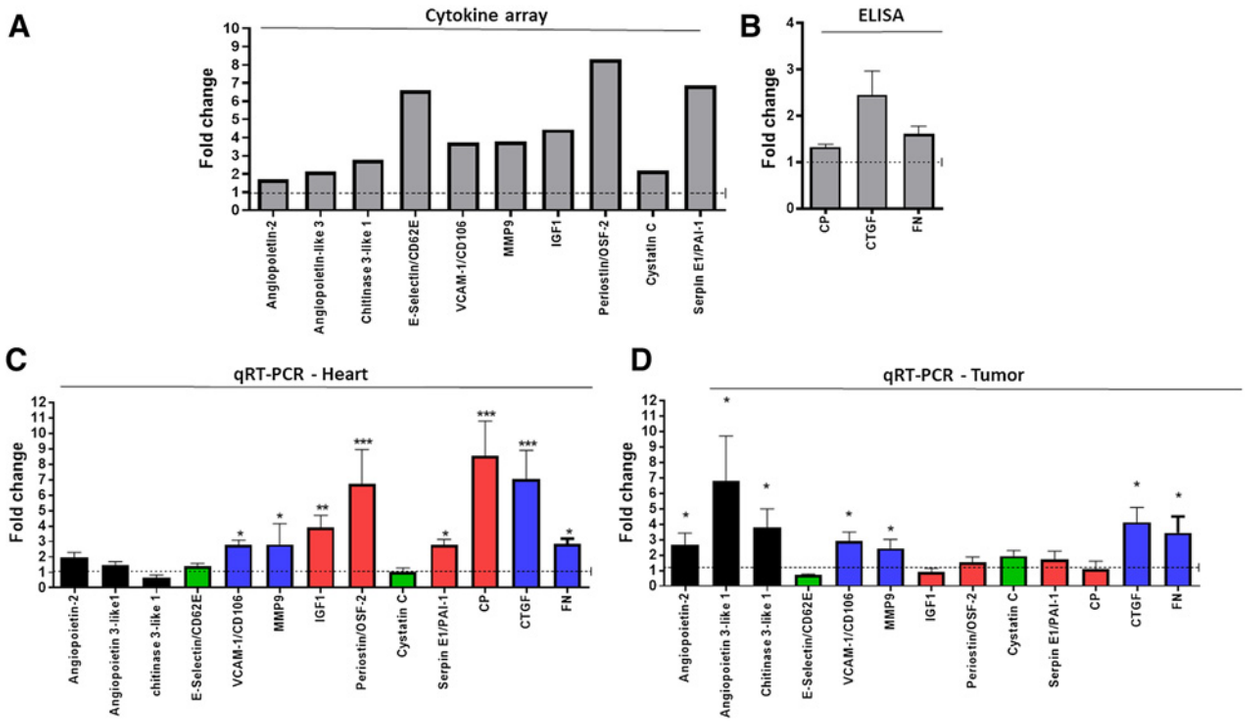

Figure 5.

Tumor progression phenotype is mediated by multiple secreted factors derived from the heart, tumor, and other tissues. **A,** Serum from either ATF3-transgenic or control mice was used to probe proteome cytokine array. For each protein, serum levels are presented as fold change relative to control serum. **B,** Serum levels as in **A**, obtained by ELISA for ceruloplasmin (CP) and CTGF and fibronectin (FN). **C** and **D,** Heart (**C**) and tumor (**D**) mRNA levels of the indicated genes were measured by qRT-PCR. Color code for the secreted factors from the heart (red), tumor (black), tumor and heart simultaneously (light blue), and other tissues and organs (green). Data are presented as mean ±SD relative expression compared with control, which was determined as 1. One-way ANOVA followed by Tukey posttests or multiple Student *t* tests. *, $P < 0.05$; **, $P < 0.01$; ***, $P < 0.001$.

skeletal muscles (48, 49), thus, further studies directed toward understanding the role of additional tissues and organs participating in a larger communication network to mediate the cross-talk between the failing heart and the tumor are needed.

Collectively, ATF3-transgenic mouse model induces spontaneous cardiac hypertrophy that promotes cancer growth and metastatic tumor characteristics. As long the cardiac damage is reversible, the cross-talk can be discontinued. However, once the hypertrophied heart mediates the cross-talk with cancer cells in an ATF3-independent manner, a vicious cycle is inevitable. This result has wide clinical implications, highlighting the importance in early diagnosis and treatment of HF prior to reaching the irreversible phase: A phase that increases cancer risk and promotes deterioration of cancer progression, aggressiveness and overall outcome.

Authors' Disclosures

A. Aronheim reports grants from Ministry of Health during the conduct of the study. No disclosures were reported by the other author.

Authors' Contributions

L. Awwad: Conceptualization, data curation, formal analysis, methodology. **A. Aronheim:** Conceptualization, data curation, formal analysis, supervision, funding acquisition, writing–review and editing.

Acknowledgments

The authors wish to thank Dr. Sharon Aviram and all members of Aronheim's lab. They wish to thank Regina Katsman for taking care of their animal colony. The authors thank Ibrahim Knani for technical help. To Prof. Dov Hershkovitz from Soraski Medical Center and Dr. Amit Avrahami for pathological advise. This work was partially supported by the Ministry of Health grant # 3-17783 (to A. Aronheim).

The costs of publication of this article were defrayed in part by the payment of page charges. This article must therefore be hereby marked *advertisement* in accordance with 18 U.S.C. Section 1734 solely to indicate this fact.

Received July 27, 2021; revised December 14, 2021; accepted March 3, 2022; published first March 8, 2022.

References

1. Ponikowski P, Anker SD, AlHabib KF, Cowie MR, Force TL, Hu S, et al. Heart failure: preventing disease and death worldwide. ESC Heart Fail 2014; 1:4–25.
2. Moslehi J, Zhang Q, Moore KJ. Crosstalk between the heart and cancer: Beyond drug toxicity. Circulation 2020;142:684–7.
3. Tocchetti CG, Ameri P, de Boer RA, D'Alessandra Y, Russo M, Sorriento D, et al. Cardiac dysfunction in cancer patients: beyond direct cardiomyocyte damage of anticancer drugs: novel cardio-oncology insights from the joint 2019 meeting of the ESC Working Groups of Myocardial Function and Cellular Biology of the Heart. Cardiovasc Res 2020;116:1820–34.

4. Koene RJ, Prizment AE, Blaes A, Konety SH. Shared risk factors in cardiovascular disease and cancer. Circulation 2016;133:1104–14.
5. Meijers WC, de Boer RA. Common risk factors for heart failure and cancer. Cardiovasc Res 2019;115:844–53.
6. de Boer RA, Hulot JS, Tocchetti CG, Aboumsallem JP, Ameri P, Anker SD, et al. Common mechanistic pathways in cancer and heart failure. A scientific roadmap on behalf of the Translational Research Committee of the Heart Failure Association (HFA) of the European Society of Cardiology (ESC). Eur J Heart Fail 2020;22:2272–89.
7. Hoshijima M, Chien KR. Mixed signals in heart failure: cancer rules. J Clin Invest 2002;109:849–55.
8. Han X, Zhou Y, Liu W. Precision cardio-oncology: understanding the cardiotoxicity of cancer therapy. NPJ Precis Oncol 2017;1:31.
9. Tocchetti CG, Galdiero MR, Varricchi G. Cardiac toxicity in patients treated with immune checkpoint inhibitors: It is now time for cardio-immuno-oncology. J Am Coll Cardiol 2018;71:1765–7.
10. Varricchi G, Marone G, Mercurio V, Galdiero MR, Bonaduce D, Tocchetti CG. Immune checkpoint inhibitors and cardiac toxicity: an emerging issue. Curr Med Chem 2018;25:1327–39.
11. Hasin T, Gerber Y, McNallan SM, Weston SA, Kushwaha SS, Nelson TJ, et al. Patients with heart failure have an increased risk of incident cancer. J Am Coll Cardiol 2013;62:881–6.
12. Hasin T, Gerber Y, Weston SA, Jiang R, Killian JM, Manemann SM, et al. Heart failure after myocardial infarction is associated with increased risk of cancer. J Am Coll Cardiol 2016;68:265–71.
13. Meijers WC, Maglione M, Bakker SJL, Oberhuber R, Kieneker LM, de Jong S, et al. Heart failure stimulates tumor growth by circulating factors. Circulation 2018;138:678–91.
14. Bertero E, Canepa M, Maack C, Ameri P. Linking heart failure to cancer. Circulation 2018;138:735–42.
15. Richards AM. Can heart failure cause cancer? Nat Rev Cardiol 2019;16:7–8.
16. Koelwyn GJ, Newman AAC, Afonso MS, van Solingen C, Corr EM, Brown EJ, et al. Myocardial infarction accelerates breast cancer via innate immune reprogramming. Nat Med 2020;26:1452–8.
17. Avraham S, Abu-Sharki S, Shofti R, Haas T, Korin B, Kalfon R, et al. Early cardiac remodeling promotes tumor growth and metastasis. Circulation 2020; 142:670–83.
18. Blau HM, Rossi MV. Tet B or not tet B: advances in tetracycline-inducible gene expression. Proc Natl Acad Sci U S A 1999;96:797–9.
19. Koren L, Elhanani O, Kehat I, Hai T, Aronheim A. Adult cardiac expression of the activating transcription factor 3, ATF3, promotes ventricular hypertrophy. PLoS One 2013;8:e68396.
20. Hai T, Wolford CC, Chang YS. ATF3, a hub of the cellular adaptive-response network, in the pathogenesis of diseases: is modulation of inflammation a unifying component? Gene Expr 2010;15:1–11.
21. Hasin T, Elhanani O, Abassi Z, Hai T, Aronheim A. Angiotensin II signaling upregulates the immediate early transcription factor ATF3 in the left but not the right atrium. Basic Res Cardiol 2011;106:175–87.
22. Zhou H, Shen DF, Bian ZY, Zong J, Deng W, Zhang Y, et al. Activating transcription factor 3 deficiency promotes cardiac hypertrophy, dysfunction, and fibrosis induced by pressure overload. PLoS One 2011;6:e26744.
23. Li Y, Li Z, Zhang C, Li P, Wu Y, Wang C, et al. Cardiac fibroblast-specific activating transcription factor 3 protects against heart failure by suppressing MAP2K3-p38 signaling. Circulation 2017;135:2041–57.
24. Kalfon R, Koren L, Aronheim A. ATF3, a novel cardiac therapeutic target: Beneficial or harmful? Int J Cardiol 2017;234:124.
25. Okamoto Y, Chaves A, Chen J, Kelley R, Jones K, Weed HG, et al. Transgenic mice with cardiac-specific expression of activating transcription factor 3, a stress-inducible gene, have conduction abnormalities and contractile dysfunction. Am J Pathol 2001;159:639–50.
26. Kistner A, Gossen M, Zimmermann F, Jerecic J, Ullmer C, Lubbert H, et al. Doxycycline-mediated quantitative and tissue-specific control of gene expression in transgenic mice. Proc Natl Acad Sci U S A 1996;93:10933–8.
27. Yu Z, Redfern CS, Fishman GI. Conditional transgene expression in the heart. Circ Res 1996;79:691–7.
28. Wolford CC, McConoughey SJ, Jalgaonkar SP, Leon M, Merchant AS, Dominick JL, et al. Transcription factor ATF3 links host adaptive response to breast cancer metastasis. J Clin Invest 2013;123:2893–906.
29. Avraham S, Korin B, Aviram S, Shechter D, Shaked Y, Aronheim A. ATF3 and JDP2 deficiency in cancer associated fibroblasts promotes tumor growth via SDF-1 transcription. Oncogene 2019;38:3812–23.
30. Saliba W, Bental T, Shapira Y, Schwartzenberg S, Sagie A, Vaturi M, et al. Increased risk of non-hematological cancer in young patients with aortic stenosis: a retrospective cohort study. Cardiooncology 2021;7:37.
31. Shi C, Aboumsallem JP, de Wit S, Schouten EM, Bracun V, Meijers WC, et al. Evaluation of renal cancer progression in a mouse model of heart failure. Cancer Commun 2021;41:796–9.
32. Kalfon R, Friedman T, Eliachar S, Shofti R, Haas T, Koren L, et al. JDP2 and ATF3 deficiencies dampen maladaptive cardiac remodeling and preserve cardiac function. PLoS One 2019;14:e0213081.
33. Palazzuoli A, Nuti R. Heart failure: pathophysiology and clinical picture. Contrib Nephrol 2010;164:1–10.
34. Wijnker PJM, Sequeira V, Kuster DWD, Velden JV. Hypertrophic cardiomyopathy: a vicious cycle triggered by sarcomere mutations and secondary disease hits. Antioxid Redox Signal 2019;31:318–58.
35. Zhao T, Su Z, Li Y, Zhang X, You Q. Chitinase-3 like-protein-1 function and its role in diseases. Signal Transduct Target Ther 2020;5:201.
36. Helfrich I, Edler L, Sucker A, Thomas M, Christian S, Schadendorf D, et al. Angiopoietin-2 levels are associated with disease progression in metastatic malignant melanoma. Clin Cancer Res 2009;15:1384–92.
37. Carbone C, Piro G, Merz V, Simionato F, Santoro R, Zecchetto C, et al. Angiopoietin-like proteins in angiogenesis, inflammation and cancer. Int J Mol Sci 2018;19:431.
38. Jassam SA, Maherally Z, Smith JR, Ashkan K, Roncaroli F, Fillmore HL, et al. CD15s/CD62E interaction mediates the adhesion of non-small cell lung cancer cells on brain endothelial cells: Implications for cerebral metastasis. Int J Mol Sci 2017;18:1474.
39. Huang H. Matrix metalloproteinase-9 (MMP-9) as a cancer biomarker and MMP-9 biosensors: Recent advances. Sensors 2018;18:3249.
40. Brahmkhatri VP, Prasanna C, Atreya HS. Insulin-like growth factor system in cancer: novel targeted therapies. Biomed Res Int 2015;2015:538019.
41. Leto G, Crescimanno M, Flandina C. On the role of cystatin C in cancer progression. Life Sci 2018;202:152–60.
42. Chu CY, Chang CC, Prakash E, Kuo ML. Connective tissue growth factor (CTGF) and cancer progression. J Biomed Sci 2008;15:675–85.
43. Kyutoku M, Taniyama Y, Katsuragi N, Shimizu H, Kunugiza Y, Iekushi K, et al. Role of periostin in cancer progression and metastasis: inhibition of breast cancer progression and metastasis by anti-periostin antibody in a murine model. Int J Mol Med 2011;28:181–6.
44. Zhang Y, Tian J, Qu C, Peng Y, Lei J, Li K, et al. Overexpression of SERPINA3 promotes tumor invasion and migration, epithelial-mesenchymal-transition in triple-negative breast cancer cells. Breast Cancer 2021;28:859–73.
45. Kwon WS, Kim TS, Nahm CH, Moon Y, Kim JJ. Aberrant cystatin-C expression in blood from patients with breast cancer is a suitable marker for monitoring tumor burden. Oncol Lett 2018;16:5583–90.
46. Dai S, Mo Y, Wang Y, Xiang B, Liao Q, Zhou M, et al. Chronic stress promotes cancer development. Front Oncol 2020;10:1492.
47. Eckerling A, Ricon-Becker I, Sorski L, Sandbank E, Ben-Eliyahu S. Stress and cancer: mechanisms, significance and future directions. Nat Rev Cancer 2021;21: 767–85.
48. Kalfon R, Koren L, Aviram S, Schwartz O, Aronheim A. ATF3 expression in cardiomyocytes preserves homeostasis in the heart and controls peripheral glucose tolerances. Cardiovasc Res 2017;113:134–46.
49. Santamans AM, Montalvo-Romeral V, Mora A, Lopez JA, Gonzalez-Romero F, Jimenez-Blasco D, et al. p38gamma and p38delta regulate postnatal cardiac metabolism through glycogen synthase 1. PLoS Biol 2021;19:e3001447.